Biomimetic jellyfish-inspired underwater vehicle actuated by ionic polymer metal composite actuators

2012 Smart Mater. Struct. 21 094026

(http://iopscience.iop.org/0964-1726/21/9/094026)

Smart Mater. Struct. **21** (2012) 094026 (11pp) doi:10.1088/0964-1726/21/9/094026

Biomimetic jellyfish-inspired underwater vehicle actuated by ionic polymer metal composite actuators

Joseph Najem[1], Stephen A Sarles[2], Barbar Akle[3] and Donald J Leo[1]

[1] Center For Intelligent Material Systems and Structures, Virginia Tech, Blacksburg, VA 24061, USA
[2] Bioinspired Materials and Transduction Laboratory, University of Tennessee, Knoxville, TN 37996, USA
[3] IME, Lebanese American University, PO Box 36, Byblos, Lebanon

E-mail: jnajem@vt.edu

Received 22 February 2012, in final form 14 June 2012
Published 31 August 2012
Online at stacks.iop.org/SMS/21/094026

Abstract
This paper presents the design, fabrication, and characterization of a biomimetic jellyfish robot that uses ionic polymer metal composites (IPMCs) as flexible actuators for propulsion. The shape and swimming style of this underwater vehicle are based on the *Aequorea victoria* jellyfish, which has an average swimming speed of 20 mm s^{-1} and which is known for its high swimming efficiency. The *Aequorea victoria* is chosen as a model system because both its bell morphology and kinematic properties match the mechanical properties of IPMC actuators. This medusa is characterized by its low swimming frequency, small bell deformation during the contraction phase, and high Froude efficiency. The critical components of the robot include the flexible bell that provides the overall shape and dimensions of the jellyfish, a central hub and a stage used to provide electrical connections and mechanical support to the actuators, eight distinct spars meant to keep the upper part of the bell stationary, and flexible IPMC actuators that extend radially from the central stage. The bell is fabricated from a commercially available heat-shrinkable polymer film to provide increased shape-holding ability and reduced weight. The IPMC actuators constructed for this study demonstrated peak-to-peak strains of ∼0.7% in water across a frequency range of 0.1–1.0 Hz. By tailoring the applied voltage waveform and the flexibility of the bell, the completed robotic jellyfish with four actuators swam at an average speed 0.77 mm s^{-1} and consumed 0.7 W. When eight actuators were used the average speed increased to 1.5 mm s^{-1} with a power consumption of 1.14 W.

(Some figures may appear in colour only in the online journal)

1. Introduction

Recent demand for autonomous underwater vehicles, such as robotic fish and even autonomous alligators in military and commercial applications motivates the design and development of new types of autonomous underwater vehicles (AUVs). AUVs have found applications in civil, commercial, and military applications [1]. Commercially, underwater vehicles are used in the oil and gas industry for seafloor mapping and surveying. AUVs are also extensively used to carry out various military tasks such as detecting underwater mines, detection of submarines, and monitoring protected areas for unidentified objects. Other uses include the study of the ocean floor and animal migration, the detection of chemical agents, and the preservation of microscopic life [1]. However, the employment of AUVs has been limited to a certain number of tasks because current technologies suffer from major limitations, such as significant maintenance requirements, high cost, and inadequate lifetime and range [1].

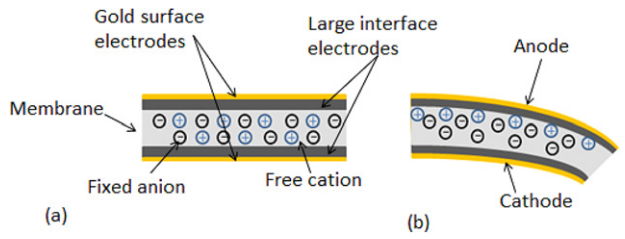

Figure 1. (a) A schematic showing the composition of an IPMC actuator along with the ions repartition in the membrane. (b) The IPMC deflects toward the cathode upon application of a voltage due to the accumulation of the free cations on the anode.

The long-term goal of our research is to design and develop a new kind of underwater vehicle that can operate over a wide surface area, in severe water conditions, and over long periods of time. Two requirements for a successful vehicle design include the ability to demonstrate proficient swimming and maneuverability in order to maintain position in water and to provide long-term and efficient use of the available energy stored on-board.

A bio-inspired engineering approach to these designs specifically focuses on translating the evolutionary successes of natural species into artificial systems that mimic the construction, function, and performance of the living system [2, 3]. To this end, our recent work has focused on developing underwater vehicles that mimic jellyfish based on their high locomotive efficiency and relatively simple design. Studies have shown that jellyfish species consume a small amount of energy compared to other aquatic species due to their low metabolic rate [4]. Moreover, due to their ability to survive in various water conditions, these species are found in almost all oceans on earth. They can be found with diameters ranging from a few millimeters to a couple of meters [5] and can be found in shallow regions and also at depths of 7000 m. Apart from that, jellyfish can adapt to different temperatures and salinity levels in water [6]. In addition to its energy efficiency and ability to survive in various environments, the morphology of the jellyfish species makes it an attractive AUV option, because its design allows payloads such as cameras, batteries and sensors to be carried.

New forms of propulsion and actuation have also been investigated for this purpose. These techniques are based on bio-inspired materials that can serve as artificial muscles that in turn can help mimic the structure, morphology and swimming behavior of the natural animal. Ionic polymer metal composites (IPMCs) are a type of electroactive material that produces mechanical deformation in response to an applied electrical field. As shown in figure 1, the IPMC, or more specifically the semi-permeable membrane, bends toward the anode upon application of an electric field. This is caused by the motion of the mobile cations within the polymer matrix [7]. As a result, IPMCs are often thought of as artificial muscles [8] and may enable a lighter weight, lower-power alternative to shape memory alloys (SMA) materials for actuating a robotic jellyfish [9].

In this paper, we discuss the bio-inspired design and development of a robotic jellyfish that features IPMC actuators. First, a study of different jellyfish species is provided. The study focuses on finding a type of jellyfish species whose propulsive properties fits the properties of IPMC actuators. Second, a bell deformation study of natural species is provided in addition to a bio-inspired bell kinematics design. Third, the design, fabrication and characterization procedures of the biomimetic robot are discussed. Finally, a discussion and analysis of the results is provided.

2. Previous work on mimicking jellyfish propulsion

Initial attempts to build robotic jellyfish have used either shape memory alloys (SMAs) [9] or ionic polymer metal composites [10–12] for providing actuation to a synthetic bell structure. In 2009, Yeom *et al* [12] developed a biomimetic jellyfish robot based on IPMC actuators. The robot did not swim freely; however a floating controller was used to maintain neutral buoyancy. Velocity measurements were presented and the maximum achieved vehicle speed was 0.057 mm s^{-1} but data on power consumption was not presented. Villanueva *et al* [9] demonstrated the fabrication of a jellyfish robot that utilized eight SMA actuators for propulsion [9]. Villanueva *et al* was able to closely mimic the swimming motion and speed of the natural jellyfish *Aurelia aurita*, but the main disadvantage of a SMA-powered jellyfish was the high power consumption required to actuate the SMA materials. The robot consumed an average and peak power of 14 W and 80 W, respectively [9].

In our previous work, a first generation robot was fabricated that featured eight radially arranged IPMC actuators within the bell structure [10]. This prototype swam vertically at an average velocity of 2.2 mm s^{-1}, while consuming an average power of 3 W [10]. However, we believe that the heavy weight of the vehicle (44 g), poor actuator performance (0.25% peak-to-peak strain), and non-biomimetic design limited the swimming ability of the initial design. A second biomimetic underwater vehicle that mimics the shape and swimming style of the *Aurelia aurita* jellyfish was designed and built [11]. The *Aurelia aurita* has an average swimming speed of 13 mm s^{-1} and is known for a high swimming efficiency. The critical components of the vehicle include the flexible bell that provides the overall shape and dimensions of the jellyfish, a central hub used to provide electrical connections and mechanical support to the actuators, and flexible IPMC actuators that extend radially from the central hub [11]. By tailoring the applied voltage waveform and the flexibility of the bell, the completed robotic jellyfish swam at a maximum speed of 1.5 mm s^{-1} and consumed 3.5 W of power [11]. For this design, we believe the uniform deformation of the robot bell was non-biomimetic since the bell deformation in a natural jellyfish is mainly concentrated toward the margin. This design did not accurately mimic the actual jellyfish and consumed more power than necessary due to a deformation pattern that did not provide for efficient propulsion. Therefore, the focus of our recent work has been to improve the robot design by better replication of the bell kinematics of the natural jellyfish.

Table 1. A table showing a comparison between prolate and oblate jellyfish species.

	Prolate	Oblate
Bell contraction	Fast	Slow
Acceleration	High	Low
Froude efficiency	Low	High
Proficiency	High	Low

3. Swimming performance and bell kinematics of different jellyfish species

In this section a study of different jellyfish species is presented in order to be able to attain a model system that best fits the properties of the IPMC actuators. As mentioned earlier, IPMC materials are soft materials and have a slow response rate [13, 14]. These properties are critical in this case because most medusae are characterized by high bell deformation and swim at frequencies that range from 0.5 to 2 Hz. Therefore the study focuses on identifying a jellyfish species that swims at a low frequency and has small bell deformation during the contraction phase.

Jellyfish species usually fall under two main categories: prolate and oblate species [15]. The differentiation between jellyfish types is directly related to the geometrical shape of the medusa's bell. Biologists frequently use the fineness ratio, which is defined as the ratio of the bell height h to its diameter d, to characterize the jellyfish swimming behavior,

$$F = \frac{h}{d}. \tag{1}$$

Prolates are characterized by high bell fineness ratio (>1.0) [16], while the oblates are characterized by a low fineness ratio (<0.5). It has been established that the swimming behavior and efficiency of medusae are highly associated with the geometry of the bell. Oblates contract their bells with a minimally moving top and a maximum bell deformation at the margin [16]. In contrast, prolates deform uniformly. These two types of deformation lead to two different types of propulsion known as jetting and rowing. Oblate species use a rowing propulsion technique to propel themselves. This technique is based on generating stopping and starting vortices during swimming. Therefore, oblates are more efficient when compared to prolates that jet water from their bells in order to swim. Table 1 shows a comparison between the oblates and prolates, demonstrating that the oblates are more efficient while the prolates are faster.

Froude efficiency is a measure of the energetic efficiency of thrust production by an organism or vehicle and is defined as follows,

$$Fr_{\mathrm{p}} = \frac{2V_{\mathrm{m}}}{V_{\mathrm{j}} + V_{\mathrm{m}}} \times 100, \tag{2}$$

where V_{m} is the velocity of the medusa, and V_{j} is the velocity of the jet. The proficiency, on the other hand, is defined as the ratio of the velocity to the bell diameter.

The goal of this work is to find species that best fit the properties (i.e. slow response rate and material properties associated with the low blocking force characteristic [17, 18]) of the IPMC actuators. Data for four different oblate species, *Aurelia aurita*, *Aequorea victoria*, *Mitrocoma cellularia* and *Phialidium gregarium,* were found in the literature. Table 2, shows a comparison between these species in terms of physiologically relevant parameters. The fineness ratio ranges shown in the table below represent the ratios associated with the contracted and relaxed phases of each species. For instance, the smallest range of 0.42–0.55 corresponds to the *Aequorea victoria* while the largest range of 0.39–0.7 corresponds to the *Mitrocoma* [16, 19]. The second criteria that we looked at were the swimming frequencies of each species. The jellyfish with the lowest swimming frequency (0.5 Hz) is the *Mitrocoma*, while the *Aequorea victoria* swims at 1.1 Hz. From this comparison we focus our attention on the *Aequorea victoria* since it has the smallest fineness ratio range, the second lowest swimming frequency and the second fastest swimming velocity [16].

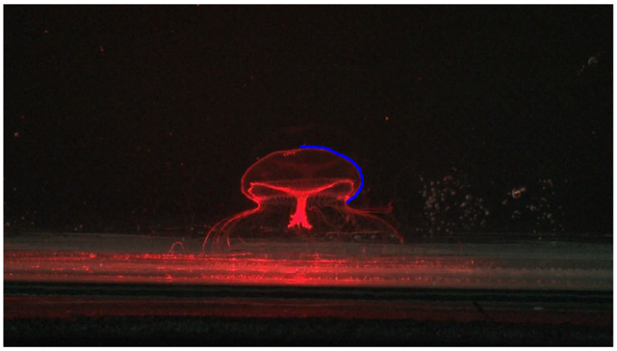

Figure 2. Image of *Aequorea victoria* specimen where its bell is fully contracted, the automatically detected points are shown as blue dots.

As previously mentioned, bell kinematics play an important role in the swimming style of the medusa. It determines the propulsion technique and thus affects the swimming speed and Froude efficiency. For this purpose an analytical and quantitative study is conducted to better understand the differences between bell deformations of both the *Aurelia aurita* and the *Aequorea victoria*. The study is narrowed down to these specific species since the *Aurelia aurita* was mimicked in first generations and by other groups and the *Aequorea victoria* is a good candidate for the project.

Videos for different swimming jellyfish species were provided by Jack Costello, Providence College and Sean Collin, Roger Williams University. The videos are converted into images using either VirtualDubMod 1.5.10.3 software or a computer vision code that is written in Matlab. Points along the bell exumbrella (the exterior side of the bell) are extracted using edge detection techniques provided by Matlab as shown in figure 2. For each frame, the coordinates at the bell summit are set to (0, 0) to be used as a reference point. This is done by subtracting the original coordinates of the apex point from all the points along the profile of the bell. This process is done at the full contraction and relaxation positions. The data is then normalized by the length of the profile for consistency.

Two methods are developed to quantitatively study the bell deformation of the natural jellyfish and the jellyfish robot.

Table 2. This table shows a comparison among four different oblate species in terms of fineness ratio range, swimming frequency, peak acceleration and peak velocity [16, 19].

	Aequorea victoria	*Mitrocoma cellularia*	*Phialidium gregarium*	*Aurelia aurita*
Fineness ratio range	0.42–0.55	0.39–0.7	0.5–0.7	0.3–0.6
Frequency (Hz)	1.1	0.5	1.67	1.67
Peak acceleration (cm s^{-2})	5	5	10	10.2
Peak velocity (cm s^{-1})	2	1.5	2.5	1.3

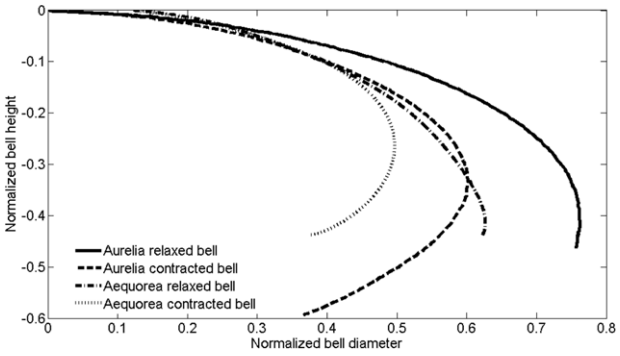

Figure 3. Relaxed and contracted bell profiles for both the living *Aurelia aurita* and the living *Aequorea victoria*.

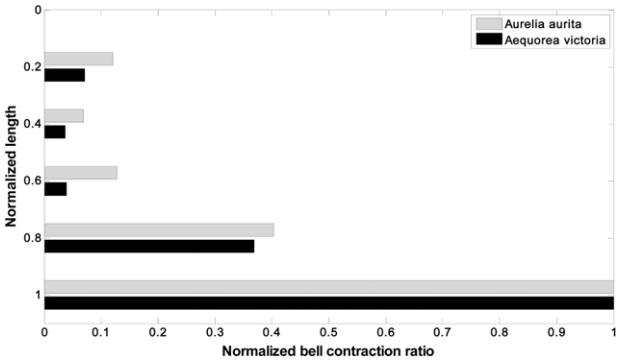

Figure 4. Normalized bell contraction of both the living *Aurelia aurita* and *Aequorea victoria* at five different points along the length of their bells.

The first method is most commonly used by biologists to quantify the deformation in natural species [15, 16]. This method consists of measuring the percentage bell contraction at five different locations along the length of the bell. The second method yields higher resolution and consists of computing the radius of curvature at different points along the length of the bell profile. This is done using a well-known approximation method called the three-points method [20]. This technique will allow us to locate the peak curvature point and to calculate the strain energy stored in the bell during the contraction phase. The combination of these methods will present a quantitative comparison between both medusae.

Figure 3 shows the bell deformation and demonstrates the difference in the bell geometry of both medusae. The *Aurelia aurita*'s bell is more flattened at the top but bends near the bell margin. In contrast the *Aequorea victoria*'s bell takes a more spherical shape, resulting in a curvature that does not exhibit any abrupt changes along the length of the bell. From previous research it was learned that the angle at which the actuator is placed affects the swimming performance of the robot [10, 11].

Figure 3 also shows the contracted bells of both jellyfishes. *Aurelia aurita*'s bell deforms along the whole length of the bell. However, this deformation is not uniform and is mainly concentrated at the end of the bell toward the margin. It is noticed also that the bell also extends during the contraction phase. On the other hand in the *Aequorea victoria* case, the bell does not deform significantly at the top, while the deformation is mainly concentrated toward the margin of the bell. The normalized bell contraction at five different points along the length of the bell profile was analyzed for both medusae to understand the differences in the deformation pattern (figure 4). The *Aequorea victoria* shows less deformation at the top part of the bell when compared to the *Aurelia aurita*. Note that the results presented refer to one position of the bell at the contraction and relaxation phases. However, different snapshots were taken and compared in order to make sure of the consistency of the results and no significant differences were noticed.

To quantify potential differences in actuation requirements we used the radius of curvature measurements to compute the normalized strain energy in the bell at maximum contraction. In a first-order approximation the bell profile is treated as a cantilever beam. Strain energy density is defined as follows,

$$U(x) = \int_{-z}^{z} \tfrac{1}{2} E \varepsilon_x^2 \, \mathrm{d}z, \tag{3}$$

where ε_x is the strain energy in the x-direction and E is the modulus of elasticity of the material. Knowing that $\varepsilon_x = z\rho(x)$ and taking $z = \frac{t}{2}$, where t is the thickness of the bell section, the overall strain energy stored in the beam becomes

$$U = \frac{Et^3}{12} \int_0^l \rho(x)^2 \, \mathrm{d}x, \tag{4}$$

where $\rho(x)$ is the curvature of the beam as a function of the beam length, and l is the beam length. The thickness and the modulus of elasticity are assumed to be the same for both bells, therefore the $\frac{Et^3}{12}$ term is dropped. As a result the data presented later refers to the $\int_0^l \rho(x)^2 \, \mathrm{d}x$ term, which we call the 'non-dimensional strain energy'. Figure 5 shows the square of the difference in curvature along the bell of the *Aurelia aurita* (solid line) and the *Aequorea victoria* (dashed line), between the relaxation and contraction phases. The peak value

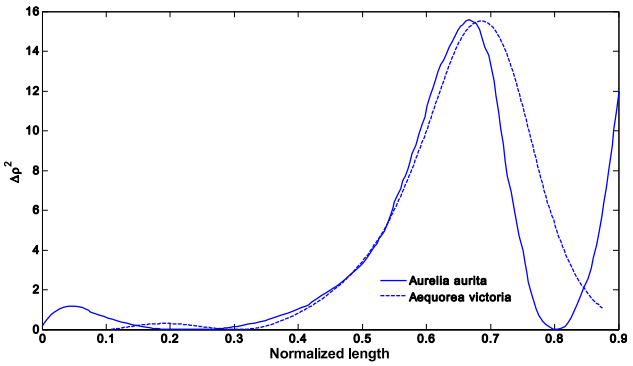

Figure 5. The square of the curvature difference at different points along the bell of the living *Aequorea victoria* and *Aurelia aurita*.

Table 3. A summary of the peak curvature and strain energy results for both medusae.

	$\triangle\rho^2$ (u^{-2}) peak values	Non-dimensional strain energy	Position (%)
Victoria	15.52	3.53	69.10
Aurita	15.58	3.84	66.60

for the curvature difference for the *aurita* occurs at 66.6% of the length of the bell, with a value of 15.58 u^{-2} and an overall strain energy of 3.84. On the other hand, the peak curvature difference seen on the bell of the *Aequorea victoria* occurs at 69% of the bell length, with a value of 15.52 u^{-2} and an overall strain energy of 3.5288. Note that since the bell length in both figures is normalized, the values obtained for the curvature difference and the total strain energy are dimensionless. Table 3 summarizes these results.

This study presents a quantitative comparison between two oblate species with a focus on their bell kinematics and morphologies. In terms of their morphologies, the results show that the *Aurelia aurita* has a more flattened shape when compared to the rounded bell shape of the *Aequorea victoria*. Previous generations of robots built by the group demonstrated that the position of the actuators underneath the bell played an important role in propulsion. Specifically, by decreasing the angle between the actuators and the neutral axis of the robot, a higher swimming speed and an increased bell deformation were achieved [10]. Since a smaller angle between the actuators and the neutral axis results in a more rounded bell shape, mimicking the morphology of the *Aequorea victoria* is more convenient for the IPMC-based jellyfish robot. This study also demonstrates the differences in the total strain energy stored in the bell and the location of the maximum curvature. The overall strain energies calculated from each species show that *Aequorea victoria* stores less strain energy in its bell than *Aurelia aurita*. Since designing a low powered robot is crucial, building a robot that mimics the bell kinematics of *Aequorea victoria* is ideal because it takes less energy to overcome the strain energy required to merely bend the bell. Based on these studies and knowing that the *Aequorea victoria* has a high Froude efficiency (95%) [16], we propose that mimicking the morphology and bell kinematics of the *Aequorea victoria* is a more appropriate match for the properties IPMC actuators and will result in a more efficient robot.

4. Fabrication and characterization of ionic polymer metal composites actuators

An ionic polymer metal composite consists of a central polymer membrane sandwiched between two conductive, high-surface-area electrodes. Application of voltage on the outer surfaces results in transverse bending due to the translocation of ions through the selective membrane [8]. The inner membrane is typically made from Nafion^{TM}, a commercially available ionomer, while the high-surface-area electrodes often consist of a blend of ionic polymer and conductive particles such as ruthenium dioxide (RuO_2), single wall carbon nanotubes (SWNT), and gold nanoparticles [11, 17]. The outer surfaces of the composites are then plated with a thin metallic layer to provide conductivity along the surface.

In this work the direct assembly process (DAP) is used to fabricate the actuators [17]. Each electrode layer is 65 μm thick and consists of a mixture of 25 vol% RuO_2, 15 vol% SWNT, 10 vol% gold nanoparticles and 50 vol% liquid Nafion. Once the electrode material is prepared, a sheet of Nafion 117 (10 cm $\times$ 7 cm) is cut and roughened using fine-grained sand paper. The electrode mixture is sprayed onto the membrane using a pneumatic paint sprayer and then the sheet is left to dry. The coated membrane is melt pressed at 210 °C and a pressure of 30 000 psi in order to bind the electrodes and the membrane together. Three layers of platinum are then applied to the electrode material using the ion impregnation method [17, 18]. Finally, the plated material is divided into equal-sized actuators and then each is gold plated using electroplating gold solution in order to increase the surface conductivity. The completed actuators made for this study are rectangular in shape (5 cm $\times$ 0.8 cm) and have a thickness of $\sim$22 μm.

The bending performance of four actuators is characterized using an apparatus that measures the deformation of the actuator and induced current due to an applied voltage. The 8 mm $\times$ 50 mm rectangular actuator is clamped with gold electrodes in a cantilevered configuration (figure 6). A sinusoidal voltage waveform is used to excite the actuators and the resulting displacement is measured with a Polytec OFV-363 laser vibrometer and a Polytec OFV-3001 vibrometer controller at a point located 20 mm from the clamped end. Two different voltage amplitudes are used (1 and 2 V) at three different frequencies (0.5, 1.0 and 2.0 Hz). A power amplifier is used to supply the voltage and current necessary for driving the actuators, while the resulting current is converted to a voltage using a non-inverting op-amp circuit. This voltage is measured using a dSPACE data acquisition system (CP1104). The free strain of the IPMC actuators is calculated according to equation (5)

$$\varepsilon(t) = \frac{\delta(t)t}{{l_f}^2}, \tag{5}$$

where $\varepsilon(t)$ is the strain, $\delta(t)$ is the measured displacement, t is the thickness of the actuator, and l_f is the free length of the

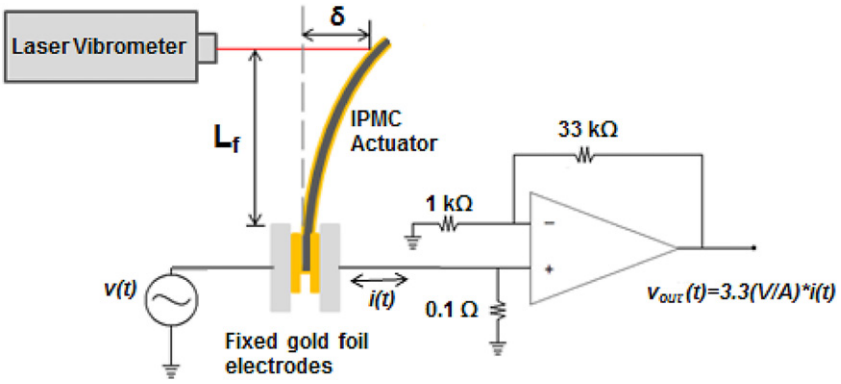

Figure 6. Schematic of the actuation characterization and current consumption measurement.

Table 4. Measured peak-to-peak strain results at 1 and 2 V and 0.5 and 1 Hz for each case.

	Peak-to-peak strain (%) results (1 V)		Peak-to-peak strain (%) results (2 V)	
Actuator	0.5 Hz	1.0 Hz	0.5 Hz	1.0 Hz
1	0.2289	0.1574	0.5866	0.3839
2	0.2889	0.1631	0.7112	0.4026
3	0.2519	0.1876	0.6312	0.4670
4	0.2420	0.1598	0.5914	0.3197

actuator. Note that the value of $x(t)$ in water is corrected by dividing it by 1.33 in order to compensate for the change in the refractive index of the laser signal crossing the air/water interface ($n_{air} = 1$, $n_{water} = 1.33$).

The measured strain of the IPMC actuators as a response of the input voltage was also computed using equation (5). The strain response varies for different actuators. Actuator 2 exhibited the highest peak-to-peak strain of 0.4026% when actuated at 1 Hz and 0.7112% when actuated at 0.5 Hz (table 4). In contrast, Actuator 3 exhibited a higher peak-to-peak strain of 0.4670% when actuated at 1 Hz; however a lower peak-to-peak strain of 0.6312% at 0.5 Hz. Actuators 1 and 4 showed similar peak-to-peak strain performance. The purpose of this study is to test and check the consistency of the bending strain percentage of the different actuators. Since their deformations are the main source of actuation for the robot, higher consistency in the bending performance of the actuators results in a more uniform bell deformation on the robot. Table 4 also shows the peak-to-peak strain response due to a 1 V voltage input.

5. Biomimetic bell kinematics design and analysis

As discussed in previous sections, the bell of an oblate medusa does not deform in a uniform way [15, 16]. The top part of the bell contracts with small deformations while the margin contracts with larger deformations. This variance in deformation in regard to its magnitude and location causes the phenomena of rowing propulsion [15]. In previous generations [10, 11] this characteristic was not taken into consideration. Rather, the IPMC actuators extended from the central hub to the margin of the bell. The consequences of such a design result in more power consumption due to the use of oversized actuators, unnecessary deformation especially in the top upper part of the bell, and a low swimming efficiency due to the failure in achieving the rowing propulsion phenomena. Therefore in order reduce the aforementioned consequences; the next step is to better mimic the bell kinematics of the real jellyfish. The following sections will discuss the design, characterization, and results of a bio-inspired bell, which mimics the morphology and kinematics of the *Aequorea victoria*.

5.1. Experimental setup

The first step was to fabricate a test structure that would mimic a radial portion of the jellyfish bell and enable testing of multiple actuator configurations. The test setup that was developed consisted of a central hub, a single IPMC actuator, a one-eighth section of a symmetric bell, and an adjustable stage that serves to change the location (x and y) and angle of the actuator that is located underneath the bell. The hub consists of two lightweight plastic halves, each having eight radially distributed gold electrode pads that are used to mechanically support and electrically connect to the IPMC actuators. The material used for the hub is ABS plastic and is printed using a rapid prototyping machine. The lightweight, flexible bell is made from polyolefin film chosen for its combination of shape-holding ability and low stiffness, which are both necessary for an IPMC-based design. The stage is made of a rectangular piece of plexiglass with equally spaced drilled holes. These holes will allow for adjusting the location of the actuator in the x-direction. The stage also allows for the inner end of the actuator to be moved vertically underneath the bell on a threaded tube that is bounded by two small nuts. Figure 7 shows the assembled experimental setup used for different experiments.

Three different actuators with similar peak-to-peak strains are used in a combinatorial fashion to understand the effect of varying the position and orientation of the actuator on bell deformation. The actuators are of different sizes: a small actuator (4.5 cm × 0.5 cm), a medium actuator (5 cm × 0.8 cm) and a large actuator (6.5 cm × 1 cm). The variation in actuator surface area enabled us to study the effect of actuator size

Table 5. Summary of the bell profile experiments for a total of 48 experiments, as well as in the last three columns the design of the experiment according to Taguchi's method (x, y and θ are shown in figure 7).

	Actuator			Design of each experiment		
	Small	Medium	Large	y	x	θ
Experiment	1	1	1	1	1	1
	2	2	2	1	2	2
	3	3	3	1	3	3
	4	4	4	1	4	4
	5	5	5	2	1	2
	6	6	6	2	2	1
	7	7	7	2	3	4
	8	8	8	2	4	3
	9	9	9	3	1	3
	10	10	10	3	2	4
	11	11	11	3	3	1
	12	12	12	3	4	2
	13	13	13	4	1	4
	14	14	14	4	2	3
	15	15	15	4	3	2
	16	16	16	4	4	1

Far
Fair
Close

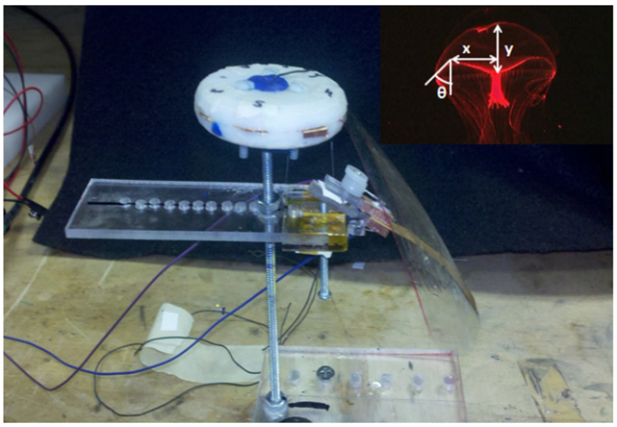

Figure 7. A picture showing the assembled experimental setup, at the top right is a picture of the actual *Aequorea victoria*, which also shows what it is meant by x, y and θ.

on power consumption. The experiment is designed using a statistical technique known as Taguchi's method [21], which utilizes three different parameters (x, y, θ) each having four different levels. As shown in table 5 (last three columns), this results in sixteen experiments for each actuator. A dSPACE digital acquisition system (CP1104) is used to provide varying voltage waveforms through a power amplifier (HP 6825) to the apparatus. The resulting motion of the IPMC actuator and the bell portion is recorded using a Motion Scope PCI 2000S (RedLake Imaging) high-speed camera and then analyzed with a computer vision Matlab code that was written in order to track the edge of the bell profile. The current consumption is also measured using a non-inverting op-amp circuit [17]. Using this measured current and the recorded voltage input, the actual electrical power consumed by the robot is computed.

Table 6. Summary of the peak curvature and strain results of the best three experiments.

Experiment	$\triangle\rho^2 u^{-2}$ peak values	Non-dimensional strain energy	Position (%)
4	7	4	64
5	10	10	65
6	10	10	65

5.2. Results

Table 5 shows the results of a total of 48 experiments. These results are distributed into three different categories: Far, Fair and Close compared to the two jellyfish species of interest. The data that we are interested in are the strain energy and the location of the point of inflection (the maximum peak point). The results in lighter color represent the Far results. Most of the results fell under this category since the bulk deformation of the ionic polymer metal composites makes it difficult to attain the exact shape. However, a few experiments fell under the Fair category since they showed reasonable results when compared to the actual animal data. The most promising results though are the ones of experiments 4, 5 and 6 which used the medium-sized actuator. Table 6 represents a summary of these results. For instance, experiment 4 shows a maximum peak curvature of 7, strain energy of 4 and a maximum peak location at 64% of the length of the bell. Experiments 5 and 6 show the exact same results. They each had a maximum peak curvature of 10, strain energy of 10 and a maximum peak location at 65% of the length of the bell. These results are promising because they are closely match the curvature and strain results of the natural jellyfish.

Due to a reduction in the size of the actuators in all three experiments, another achievement in all three experiments was a power reduction. Figure 8 shows the power

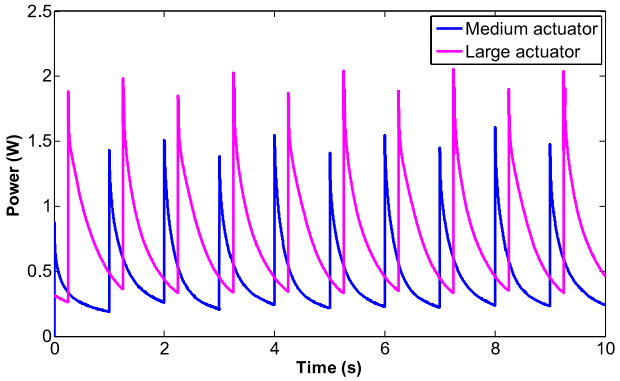

Figure 8. Power consumption results comparison between the large and the medium actuators.

consumption of the large and medium size actuators. It is shown that the power is reduced by 40% when the size of the actuator is reduced by ∼39% from 6.5 cm^2 (large actuator) to 4.0 cm^2 (medium actuator).

6. Biomimetic jellyfish robot mimicking *Aequorea victoria*

The results in the previous section describe our rationale and approach for focusing on the *Aequorea victoria* as a model system for a biomimetic robot. The resulting biomimetic jellyfish consists of four parts: a central hub, eight equally distributed spars, a stage, the IPMC actuators, and a flexible bell. The hub is made of two, lightweight plastic halves. The top half is T-shaped where the horizontal disc represents the hub and the vertical tube represents the portion at which the stage will be attached. The stage will be able to move along the tube by inserting into holes along the structure. The bottom part is a simple circular hub. The material used for the hub is ABS plastic and is printed using a rapid prototyping machine. Figure 9(a) shows the CAD models of the top and bottom parts of the hub, the spars, and the connector assembled together. The purpose of these spars is to keep the top part of the bell stationary during the contraction phase. These spars also add stability to the submerged robot. The stage is the central body that holds the IPMC actuators; it consists of a main part and eight similar clamps. Figure 9(a) shows the CAD models of the assembled parts. The gold electrodes are fabricated with gold foil (Arrow Springs, 23 kt, 65 g m^{-1}) and are wired such that contacts on the lower and upper hubs are wired in parallel, as illustrated in figure 9(b). This wire arrangement is chosen such that all eight IPMCs are actuated simultaneously. The lightweight, flexible bell is made from polyolefin film, chosen for its combination of shape-holding ability and low stiffness. The mold used to shape the bell mimics the geometry of the *Aequorea victoria* jellyfish. Finally, eight IPMC actuators (each 5 cm × 0.8 cm) are sandwiched between the two halves of the eight distinct clamps and extend radially outward from the stage. The free end of each actuator is held by a horizontal sleeve on the underside of the bell. The final weight of the robot is approximately 20 g and has an overall diameter of 15 cm and a height of 5.8 cm. The assembled biomimetic jellyfish is shown in figure 10(a).

The free-swimming performance of the IPMC-based jellyfish is studied in a 50 cm × 45 cm × 70 cm aquarium filled with water (figure 10(b)). A dSPACE digital acquisition system (CP1104) is used to provide varying voltage waveforms through a power amplifier (hp 6825) to the jellyfish. The resulting motion of the robot is recorded using a Motion Scope PCI 2000S (RedLake Imaging) high-speed camera and then analyzed with Motion Trace software to trace specific regions of the jellyfish during swimming. The current consumption is also measured using a non-inverting op-amp circuit [17]. Together with the recorded voltage input, the actual electrical power consumed by the robot is computed. Note that during free-swimming tests, counter weights (a maximum of 2 g) are attached to the hub of the robot in order to adjust the buoyancy of the jellyfish. The robot is actuated by four actuators for the first set of experiments and eight for the second set. For each set of experiments the position of the actuators was varied in the *y*-direction between 1.5 and 2 cm. At each actuator position, two bell configurations were tested (full bell and half-way cut bell), and for each configuration, a square waveform voltage is applied at different frequencies and with different duty cycles. The asymmetric square wave was inspired by the natural jellyfish that contracts its bell in an asymmetric way. The relative durations of the power and relaxation strokes are different, where the power stroke is shorter. This duration difference between both strokes is responsible of the forward motion of the medusa.

Figure 11(a) shows an example of an input voltage waveform to the robot. A particular signal which consisted of a square wave with different duty cycles was used when testing the swimming ability of the robot. In this study, the voltage amplitude was held constant at 2 V (4 V peak-to-peak), and the duty cycle of the square wave was

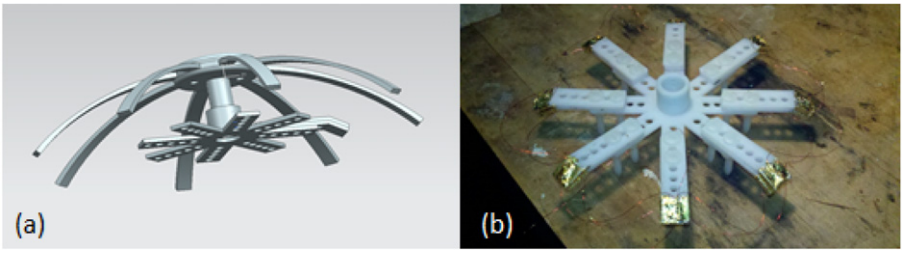

Figure 9. (a) CAD model showing the assembly of all parts of the robotic jellyfish. (b) A photograph showing the central stage, the clamps and the electrical connections.

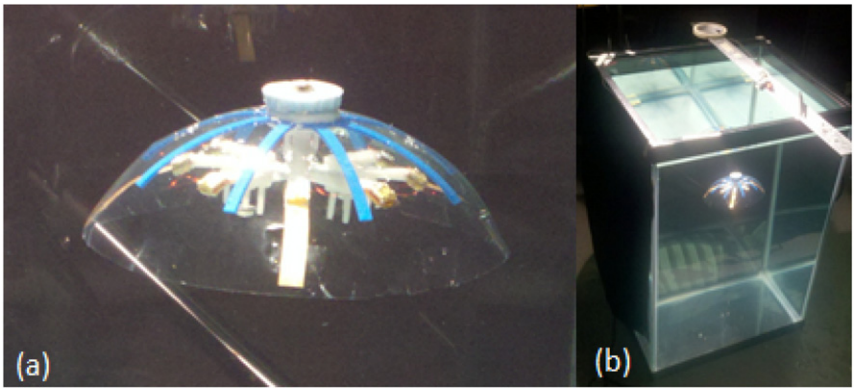

Figure 10. (a) A picture of the assembled jellyfish robot. (b) A picture of the experimental setup.

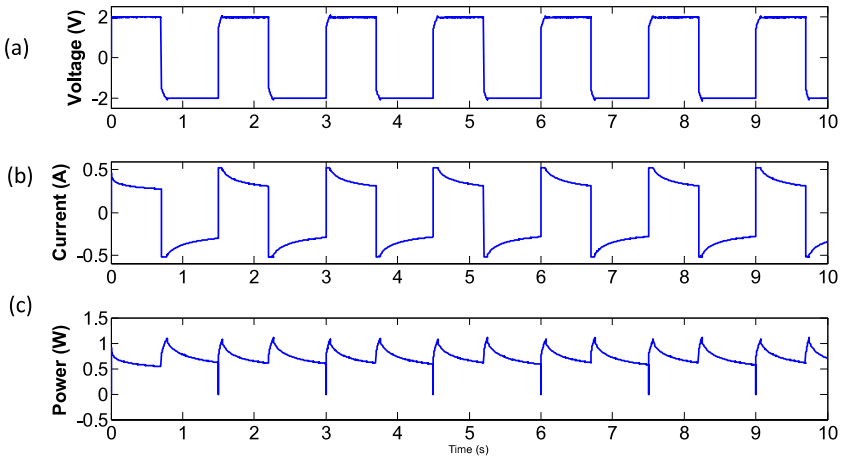

Figure 11. (a) The input voltage used to actuate the robotic jellyfish, (b) the current consumption of the robotic jellyfish, and (c) the power consumption of the robotic jellyfish.

varied from 30% to 50%. The current consumption of the robotic jellyfish for the applied voltage shown in figure 11(a) was also measured and is shown in figure 11(b). The power consumption is thus computed using measured values of the applied voltages and resulting currents. The average power consumption for the jellyfish was 0.7 W when four actuators were used and 1.14 W when eight actuators used. Note that both the current and power consumption varied with the variation of the duty cycle. The resulting motion of the jellyfish also depended on the applied voltage waveform. Basically, the power consumption is due to both electrical losses and the IPMC actuators. The electrical losses are minimized by using low resistance and short wires and covering the electrodes with gold to increase conductivity. On the other hand the power can be controlled by the size, number and position of the IPMC actuators, which will in turn affect the swimming behavior of the robot.

Our results demonstrated that the net motion of the robot changed as the duty cycle was varied. Figure 12 shows a 3D plot of the velocity of the jellyfish as a function of both the frequency and the duty cycle. Akle *et al* [10] also demonstrated that an asymmetric square wave (45% duty cycle) achieved the maximum swimming speed with the first-generation robot. One limitation of using IPMC materials for actuating the jellyfish is that their relatively low stiffness and blocked force (0.74 N m^{-1} and 20 MPa, respectively [13, 14]) limits thrust. This constraint was overcome by using a bell material that is highly flexible but which can also maintain the undeformed bell geometry. Using a heat-shrinkable polyolefin film, a lightweight flexible bell was molded to mimic the shape of *Aequorea victoria* jellyfish.

As a method for reducing the bending stiffness of the molded bell, radial cuts positioned between actuators and extending from the outer perimeter in toward the hub are introduced. A similar approach was used by Villanueva *et al* for increasing the swimming speed and actuation profile of the SMA-actuated biomimetic jellyfish [9]. Two sets of swimming tests were performed to understand this effect of bell geometry and stiffness: a bell with no cut and a bell with cuts that extend half-way from the outer edge to the hub. Figure 13 shows the vertical displacement of the jellyfish robot during a 30 s actuation period for four different configurations of the robot at 2 V. The traces exhibit an oscillatory motion corresponding to the frequency of the applied waveform and demonstrate that the jellyfish swam upwards. When no cuts are introduced to the bell the robot swims at slower velocities due to the increase in mechanical resistance of the bell. When the cuts are introduced to the

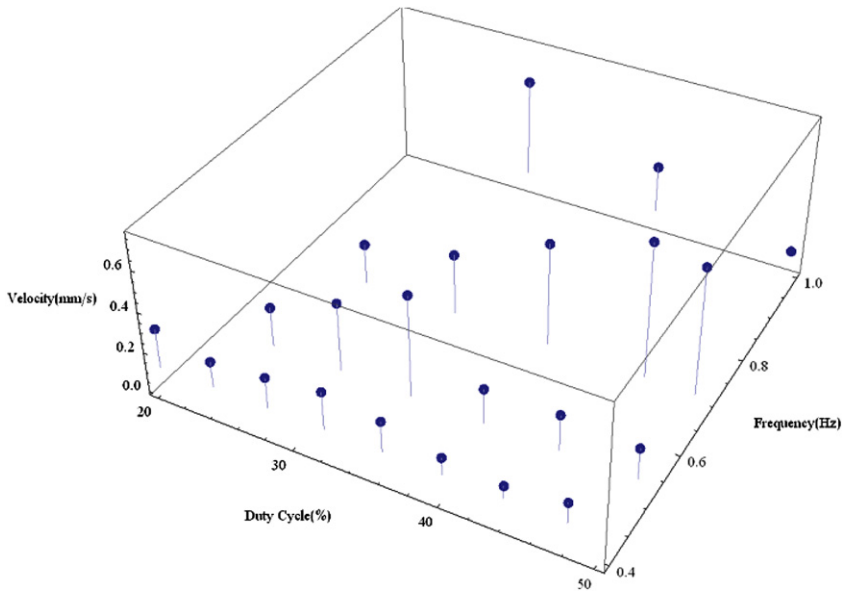

Figure 12. A 3D plot showing the velocity of the jellyfish with four actuators used as a function of frequency and duty cycle, the velocities are in mm s^{-1}.

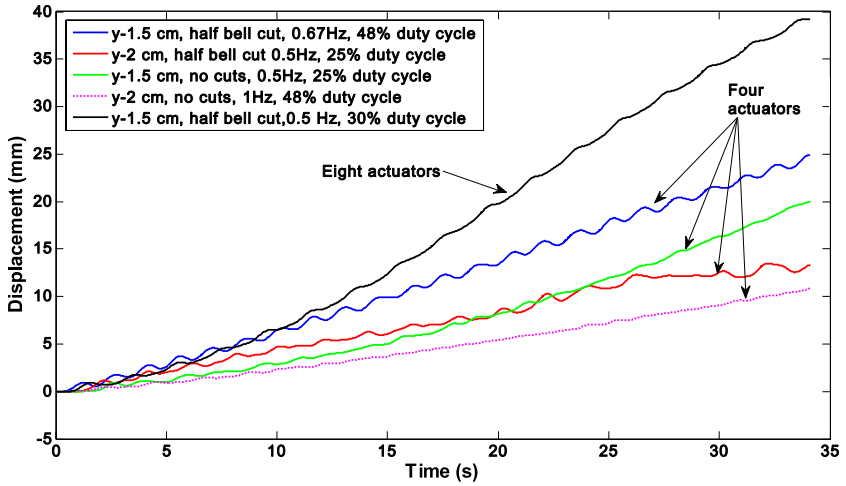

Figure 13. The vertical displacement of the jellyfish for different configurations using four and eight actuators.

Table 7. A summary of the swimming frequency, duty cycle and speed of the robot along with the power consumption for the four different configurations.

	Bell	Frequency (Hz)	Duty cycle (%)	Average speed (mm s^{-1})	Average power (W)
1.5 cm	Half-cut	0.67	46.67	0.77	0.7
	No-cuts	0.67	33.33	0.72	0.65
2 cm	Half-cut	0.5	25	0.4	0.55
	No-cuts	1	45.45	0.36	0.79

bell, the performance of the robot improved. When half-way cuts are introduced, the robot swam faster with an oscillation frequency similar to the uncut bell. Figure 13 also shows the results for two different positions of the stage at 1.5 and 2 cm from the hub. The results shown in table 7 also show that the robot swims faster when the stage is positioned at 1.5 cm. Finally figure 13 also shows the vertical displacement for the robot when eight actuators are used. This robot swam at a speed equal to ∼1.5 mm s^{-1} and consumed 1.14 W.

7. Conclusion

This paper presents the design and development of a biomimetic jellyfish robot utilizing IPMC actuators as the

propulsive mechanism. The robot is able to swim freely at a maximum speed of 1.5 mm s^{-1} at an average power consumption rate of 1.14 W if eight actuators are used and 0.77 mm s^{-1} and consumed 0.7 W when four actuators are used. It is shown that the swimming speed and power consumption is dependent on the bell geometry, input wave form duty cycle and frequency. The modular design presented in this paper enabled a schematic investigation of the design parameters to understand their effect on vehicle performance. The bio-inspired design of the bell kinematics, specifically shifting the position of the actuator forming the hub and reducing the size of the actuator, significantly improved the performance of the robot by reducing the power by 70% compared to the last *Aurelia aurita* robot jellyfish generation.

Acknowledgment

The authors would like to acknowledge the financial support offered through Office of Naval Research MURI (N000140810654).

References

[1] Wernli R L 2002 AUVs—a technology whose time has come *Proc. 2002 Int. Symp. on Underwater Technology*
[2] Franceschini N, Ruffier F and Serres J 2007 A bio-inspired flying robot sheds light on insect piloting abilities *Curr. Biol.* **17** 329–35
[3] Leitão P 2008 A bio-inspired solution for manufacturing control systems *Innovation in Manufacturing Networks* ed A Azevedo (Boston: Springer) pp 303–14
[4] Seibel B A and Drazen J C 2007 The rate of metabolism in marine animals: environmental constraints, ecological demands and energetic opportunities *Phil. Trans. R. Soc.* B **362** 2061–78
[5] Omori M 2004 Taxonomic review of three Japanese species of edible jellyfish (Scyphozoa: Rhizostomeae) *Plankton Biol. Ecol.* **51** 36
[6] Purcell J E 2005 Climate effects on formation of jellyfish and ctenophore blooms: a review *J. Mar. Biol. Assoc. UK* **85** 461
[7] Bennett M D *et al* 2006 A model of charge transport and electromechanical transduction in ionic liquid-swollen Nafion membranes *Polymer* **47** 6782–96
[8] Shahinpoor M 1998 Ionic polymer–metal composites (IPMCs) as biomimetic sensors, actuators and artificial muscles—a review *Smart Mater. Struct.* **7** R15–30
[9] Villanueva A, Smith C and Priya S 2011 A biometric robotic jellyfish (Robojelly) actuated by shape memory alloy composite actuators *Bioinspir. Biomim.* **6** 036004
[10] Akle B *et al* 2011 Design and development of bio-inspired underwater jellyfish like robot using ionic polymer metal composite (IPMC) actuators *Proc. SPIE* **7976** 797624
[11] Najem J 2011 Design and development of a biomimetic jellyfish robot that features ionic polymer metal composites actuators *Proc. SMASIS, Conf. on Smart Materials Adaptive Structures and Intelligent Systems*
[12] Yeom S-W 2009 A biomimetic jellyfish robot based on ionic polymer metal composite actuators *Smart Mater. Struct.* **18** 085002
[13] Akle B J *et al* 2005 Correlation of capacitance and actuation in ionomeric polymer transducers *J. Mater. Sci.* **40** 3715–24
[14] Akle B 2007 Development and modeling of novel extensional ionic polymer transducers *Proc. SPIE—Int. Soc. Opt. Eng.* **6524** 652411
[15] Colin S P 2002 Morphology, swimming performance and propulsive mode of six co-occurring hydromedusae *J. Exp. Biol.* **205** 427
[16] Costello J H 2000 Kinematic comparison of bell contraction by four species of hydromedusae *Sci. Mar.* **64** 47
[17] Akle B *et al* 2007 Direct assembly process: a novel fabrication technique for large strain ionic polymer transducers *J. Mater. Sci.* **42** 7031–41
[18] Kim K J 2003 Ionic polymer metal composites: II. Manufacturing techniques *Smart Mater. Struct.* **12** 65–79
[19] Costello J H and Colin S P 1994 Morphology, fluid motion and predation by the scyphomedusa *Aurelia aurita*, *Mar. Biol.* **121** 327–34
[20] Williams D J and Shah M 1992 A fast algorithm for active contours and curvature estimation *CVGIP: Image Underst.* **55** 14–26
[21] Roy R K 2010 *A primer on the Taguchi Method* (Dearborn, MI: Society of Manufacturing Engineers)